RSC Applied Polymers

ROYAL SOCIETY OF CHEMISTRY

PAPER

View Article Online
View Journal | View Issue

Cite this: *RSC Appl. Polym.*, 2026, **4**, 363

Challenging the status quo: recyclability and performance of wood fiber thermoplastic composites

Luis Valencia, *[a] Erik Persson,[a] Daniel Tano,[a] Ramón Díaz de Leon,[b] José Alejandro Díaz,[b] Ricardo Mendoza,[b] Francisco Javier Enríquez-Medrano,[b] Simone Sala,[c] He Li,[d] Francisco Vilaplana[d] and Mikael Skrifvars[e]

We present a systematic study of thermoplastic polypropylene (PP) composites reinforced with wood fibers (WF) derived from Norway spruce industrial residues (FibraQ) as scalable, sustainable alternatives to conventional polymers. The wood fibers retain a characteristic softwood monosaccharide profile and display robust morphological integrity and uniform dispersion across loadings from 20 to 50 wt%. Mechanical characterization demonstrates a linear increase in tensile modulus and strength with increasing WF content, counterbalanced by reduced ductility and impact toughness due to increasing fiber network density. Thermal analyses confirm enhanced stability and elevated Vicat softening temperatures upon WF addition. Importantly, these composites exhibit outstanding closed-loop mechanical recyclability: after three industrially relevant processing cycles, PPWF retains >90% of initial stiffness and >94% tensile strength, significantly outperforming neat PP and previously reported biocomposite systems. Our study provides the first direct quantitative comparison of recyclability and structural retention for industrially relevant PPWF composites. These advances offer a pathway for integrating renewable residues into high-performance, durable, and circular materials platforms beyond the capabilities of conventional polymers.

Received 21st October 2025,
Accepted 30th November 2025

DOI: 10.1039/d5lp00332f

rsc.li/rscapplpolym

1. Introduction

The global plastics crisis – with annual production exceeding 400 million tons[1–4] and recycling rates stagnating below 9% [5,6] – has intensified efforts to develop circular bioeconomy solutions.[7–9] Wood processing residues offer a critical yet underutilized resource in this transition, with 1.3 billion tons of lignocellulosic byproducts generated annually worldwide.[10] In Northern Europe alone, Norway spruce (*Picea abies*) processing yields 14.6 million tons of industrial residues annually, where 60–80% face low-value applications like boiler fuel despite their potential as high-performance material feedstocks.[11]

Natural fiber-reinforced polymer composites (NFPCs) represent a promising class of materials that can replace conventional plastics in automotive, furniture, and packaging applications. Their appeal stems from the biogenic origin of the natural fibers, which can significantly lower the carbon footprint and environmental impact of composite products. Market analysis projects the global natural fiber composites sector to reach nearly $12 billion by 2030, driven by sustainability mandates, consumer demand, and tightening environmental regulations.[12,13] Policy frameworks such as the European Union's Circular Economy Action Plan and Bioeconomy Strategy further underscore the importance of integrating biomass and bio-based products into circular value chains, while emphasizing the need for improved eco-design, recycling, and material safety.[14]

Recent advancements in NFPCs have focused on improving interfacial adhesion through fiber treatments (*e.g.*, alkali, silane) and matrix functionalization with compatibilizers like maleic anhydride-grafted polypropylene (MAPP).[15–17] Hybrid composites combining natural fibers with glass or carbon fibers have shown enhanced mechanical performance, while surface-modified nanocellulose additives improve thermal stability.[18–20]

Importantly, recent research efforts have increasingly addressed the recycling of NFPCs, recognizing it as a critical

[a]*Greewave AB, Skrikarhyttan 116, 71392 Gyttorp, Sweden. E-mail: luisalex_val@hotmail.com*
[b]*Research Center for Applied Chemistry, Blvd Enrique Reyna 140, 25294 Saltillo, Mexico*
[c]*Division of Materials and Production, RISE Research Institutes of Sweden, Scheelevägen 17, 223 70 Lund, Sweden*
[d]*Division of Glycoscience, Department of Chemistry, KTH Royal Institute of Technology, AlbaNova University Centre, Roslagstullsbacken 21, 10691 Stockholm, Sweden*
[e]*Swedish Centre for Resource Recovery, Faculty of Textiles, Engineering and Business, University of Borås, 501 90 Boras, Sweden*

and underexplored aspect of their sustainability and scalability. Studies have demonstrated mechanical recycling protocols for NFPCs that retain a high percentage of stiffness and strength over multiple processing cycles, often leveraging compatibilizers to enhance fiber–matrix adhesion and reduce degradation during melt processing.[21–23] Advanced chemical recycling strategies and sorting technologies have also emerged as promising approaches to overcome the challenges posed by composite heterogeneity and mixed-material streams.[24]

However, widespread adoption is impeded by several systemic barriers: (i) the logistical inefficiency and need for specialized process equipment with low-bulk-density wood residues undermine their economic viability and increase associated carbon emissions-challenges partially addressed in this work through the use of pelletized FibraQ format (bulk density 500 kg m^{-3}); (ii) the hydrophilic nature of wood fibers (WF), which compromises interfacial adhesion with hydrophobic polymer matrices, limiting mechanical performance and durability; (iii) the absence of established recycling streams and uncertainty in material value chains, which disincentivizes recovery efforts and limits circularity, as conventional recycling infrastructure is poorly adapted to composite materials-the primary focus of this study, with quantitative evidence provided in Table 3 and Fig. 11 establishing viable re-

Fig. 1 Production and applications of wood fiber pellets in biocomposites: (a) schematic representation of the circular value chain: sustainably managed spruce forests provide processing residues that are densified and pelletized to yield standardized wood fiber pellets, which are subsequently screened to remove fines, and compounded into biocomposite materials for commercial product manufacturing. (b–d) Examples of injection-molded products produced from wood fiber composite formulations; (c) component part illustrating a rigid polypropylene/wood fiber structure overmolded with a thermoplastic elastomer (TPE). (e) Large-format additive manufacturing demonstrated by the fabrication of a full-size, 3D-printed (FDM) kayak from wood fiber-reinforced recycled plastics, developed in partnership with RISE Research Institutes of Sweden and Melker of Sweden using FibraQ.[26]

cycling pathways and density-based sorting windows; (iv) moreover, the dustiness of loose wood fibers presents significant explosion hazards under ATEX (explosive atmosphere) regulations, particularly when fine particulates are present at concentrations above critical thresholds-eliminated through the pelletized FibraQ feedstock with <1% dust content (Table 1); and (v) the inherent processability challenges stemming from significant variations in fiber dimensions, morphology, and surface properties between batches, seasons, and geographic origins, which create unpredictable rheological behavior during melt processing and compromise quality control in industrial manufacturing environments-addressed through standardized pelletized feedstocks with controlled fiber dimensions and chemical composition.

To overcome persistent challenges in natural fiber-reinforced composites—namely low bulk density, poor interfacial adhesion, limited recyclability, and safety risks—this study evaluates a standardized wood fiber in pellet format[25] optimized for thermoplastic compounding commercialized by Greewave AB. We systematically investigate polypropylene (PP) composites reinforced with varying loadings of industrially sourced wood fibers, focusing on their mechanical performance, thermal properties, and quantitative evaluation of closed-loop mechanical recyclability over multiple processing cycles—the primary experimental contribution of this work and a critical and underexplored aspect for scalability and circularity in biocomposites. By linking fiber morphology, network evolution, and material durability, our work provides quantitative evidence demonstrating superior retention of mechanical properties post-recycling compared to neat PP and establishes practical density-based sorting strategies, advancing the development of high-performance, recyclable biocomposites from wood-based residues to support the transition toward circular materials systems.

2. Methods

2.1. Materials

Wood fibers (FibraQ), in the form of pellets were produced by Greewave AB (Sweden) and used as received. Commercial polypropylene (PP, Moplen EP249R, MFI = 25 g per 10 min at 230 °C per 2.16 kg) was sourced from LyondellBasell (Netherlands) and used as the matrix polymer. Maleic anhydride-grafted polypropylene (MAPP) was used as a compatibilizer, and the grade was BYK 8112 and was sourced from BYK.

Table 1 General properties of the wood fibers used in this study

Property	Value/range
Wood species	Norwegian spruce
Format	Pellets
Pellet size (diameter × length)	4 × 5 mm
Bulk density of pellets[a]	500 kg m^{-3}
Moisture content[b]	5–7%
Dust content	<1%
Mechanical durability[c]	93%

[a] Bulk density was measured by gravimetric method following ISO 17828. [b] Moisture content by oven-dry method (EN ISO 18134-1). [c] Mechanical durability was evaluated using EN 15210-1.

2.2. Methods

2.2.1. Composite preparation. Prior to processing, both PP and wood pellets were dried at 80 °C under vacuum for 4 hours to remove residual moisture. Composites containing 20, 30, 40 and 50 wt% of wood fibers, and 2% MAPP, were prepared by melt compounding in a co-rotating twin-screw extruder (Brabender, L/D = 40). Despite having a relatively short length-to-diameter ratio, the extruder design (such as the mixing notches in the metering section) allows for longer residence times compared to extruders with twice the length. The extruder was operated at a barrel temperature of 180 °C and a screw speed of 60 rpm. The extruded strands were air-cooled and subsequently pelletized.

The composite pellets were subsequently injection molded (Nissei FXN80) into standard test specimens including ASTM D638 tensile bars and ASTM D256 impact test specimens. Injection molding parameters were barrel temperature profile of 175–180–190–195–190 °C (feed to nozzle), mold temperature of 40 °C, injection pressure of 853 bar, and cooling time of 18 seconds.

2.2.2. Recyclability study. For recyclability studies, molded specimens were tested for mechanical properties, then shredded using an Arthur Thomas knife mill equipped with a 1/4-inch screen, and reprocessed following identical extrusion and injection molding parameters for up to three complete processing cycles, (mechanical recyclability was evaluated by subjecting virgin materials to multiple processing cycles). After each cycle, standardized test specimens were manufactured and characterized for mechanical, thermal, and morphological properties. The percentage retention of key mechanical properties was calculated relative to the virgin composite values.

2.3. Characterization

2.3.1. Fiber analysis and microscopic evaluation. The physical properties of the fiber pellets were measured following established or adapted standards where available: bulk density by gravimetric method similar to EN ISO 17828, moisture content by oven-dry method (EN ISO 18134-1). Mechanical durability was evaluated using EN 15210-1. Fiber dimensions and dispersion were analyzed *via* optical microscopy and scanning electron microscopy (SEM). For optical analysis, molded specimens were examined under transmitted light using an Olympus BX53 microscope equipped with a digital camera. For SEM images, a JEOL 7000 scanning electron microscope operated at an acceleration voltage of 2 kV. Specimens were mounted on aluminum stubs, and sputter-coated with gold for 30 seconds prior to observation.

2.3.2. Mechanical testing. Tensile properties were determined according to ISO 527 using an Instron 4204 universal testing machine equipped with a 10 kN load cell. Tests were

conducted at a crosshead speed of 5 mm min^{-1}. Young's modulus, tensile strength, and elongation at break were recorded. A minimum of five specimens per composition were tested, and average values with standard deviations were reported.

Flexural properties (flexural strength and modulus) were measured following ISO 178 in three-point bending configuration using the same Instron machine at a crosshead speed of 2 mm min^{-1} and a span length of 64 mm.

Impact strength of the biocomposites as a function of wood share (Fig. 7) was measured using the Charpy impact method on unnotched specimens. The measurements were carried out with a CEAST 9050 pendulum impact tester equipped with a 2.75 J hammer, under controlled room temperature conditions.

Impact strength during the recyclability study (Table 3) was determined according to ASTM D256 using the same CEAST 9050 pendulum impact tester with a 2.75 J hammer. Notched Izod specimens (63.5 × 12.7 × 3.2 mm^3), featuring a 2.54 mm deep notch, were tested at room temperature.

2.3.3. Physical properties. Melt Flow Index (MFI) was measured according to ISO 1133 (230 °C per 2.16 kg) using a Göttfert MI-4 plastometer to assess the rheological changes induced by repeated processing. This parameter provides critical information about the processability of the composites.

Density measurements were performed using the water displacement method according to ISO 1183-1.

To evaluate recyclability-related density-based separation potential, dried specimens were subjected to flotation tests in water. Specimens were first dried at 90 °C for 1 hour, weighed, and then fully immersed in water-filled containers. The floating/sinking behavior was documented photographically. The critical wood fiber content for submersion was determined by correlating calculated composite densities with experimental observations.

2.3.4. Thermal analyses. Thermogravimetric analysis (TGA) was performed using a TA Instruments Q50 analyzer to assess thermal stability and decomposition behavior. Samples (10 ± 0.5 mg) were heated from room temperature to 600 °C at a heating rate of 10 °C min^{-1} under a nitrogen atmosphere (50 mL min^{-1} flow rate). Weight loss and derivative weight loss (DTG) curves were recorded to identify decomposition temperatures and rates for virgin and recycled materials.

Differential scanning calorimetry (DSC) was conducted on a TA Instruments Model 2000 calorimeter. Samples (5–7 mg) were sealed in aluminum pans and subjected to a heat-cool-heat cycle: heating from room temperature to 200 °C at 5 °C min^{-1}, holding for 5 minutes to erase thermal history, cooling to 30 °C at 10 °C min^{-1}, and reheating to 200 °C at 5 °C min^{-1}. All measurements were performed under nitrogen atmosphere (50 mL min^{-1}). Melting temperatures (T_m) were determined from the second heating curve.

Vicat softening temperature (VST) was measured according to ISO 306 Method B using a Coesfeld HDT/Vicat testing machine with a heating rate of 50 °C h^{-1} and 50 N load.

2.3.5. Chemical composition analysis. For monosaccharide composition, 1 mg of wood fibers was hydrolyzed with 125 µL of 72% (w/w) H_2SO_4 at room temperature for 3 h, then diluted with 1375 µL Milli-Q water and further hydrolyzed at 100 °C for 3 h. Hydrolysates were spiked with 1 mg mL^{-1} inositol (internal standard), diluted 1 : 10 with MilliQ water, and filtered through 0.45 µm Chromacol syringe filters. High-performance anion-exchange chromatography with pulsed amperometric detection (HPAEC-PAD, Dionex ICS-6000, CarboPac PA20, 30 °C, 0.4 mL min^{-1}) was used to separate and quantify individual monosaccharides, employing appropriate elution gradients for neutral and acidic sugars.

The surface chemical composition of the fibers was measured by X-Ray Photoelectron Spectroscopy (XPS), using a Riber LDM-32 spectrophotometer. An aluminum anode was used, operating at 150 W with a step of 20 eV for the individual photoelectron lines. For the deconvolution of the C 1s signal, a fit was made using Shirley background subtraction and a series of Voight peaks.

2.3.6. Synchrotron-based micro-computed tomography. Three-dimensional fiber distribution was characterized by micro-computed tomography (µCT) performed at the European Synchrotron Radiation Facility (ESRF, France) on beamline BM05. Phase-contrast tomography was employed to enhance contrast between the wood fibers and polymer matrix. 58 volumes – each 1.5 × 1.5 × 1.5 mm^3 – were scanned from 3 sample types. Tomographic reconstruction was carried out *via* Paganin phase retrieval leading to reconstructed volumes with 0.729 µm isotropic voxel size. Volumes were further segmented to locate PP and wood fibers based on thresholding. Then, the volume fraction of wood fiber within each tomogram (*i.e.* horizontal 2D virtual slice through a volume) was computed for all available volumes (*i.e.* stacks of tomograms).

3. Results and discussion

3.1. Wood fibers

This study assessed wood fibers (in pelletized format) derived from industrial Norwegian spruce (*Picea abies*) residues to investigate their suitability as reinforcements in thermoplastic composites. The pellets were characterized by controlled dimensions (4 × 5 mm), increased bulk density (500 kg m^{-3}), low dust content (<1%), and high mechanical durability (93%), enabling efficient dosing, handling, and thermomechanical processing. These properties are summarized in Table 1.

The compatibility of wood fiber pellet-based composites with conventional polymer processing technologies is illustrated through previously reported demonstrator applications developed using Greewave AB's material FibraQ and partners, these include injection-molded consumer products with complex geometries (Fig. 1b), multi-material parts where rigid wood fiber/polypropylene structures are overmolded with thermoplastic elastomers (TPE) (Fig. 1c), and automotive components (Fig. 1d). Furthermore, successful large-format additive manufacturing was demonstrated by fabricating a full-size kayak from fiber-reinforced recycled polymer blends (Fig. 1e), as reported in publicly available sources,[26] highlighting scal-

ability for advanced design and manufacturing applications. Application development for these products was performed through industrial feedback regarding performance requirements and processing parameters.

3.1.1 Fiber morphology. The reinforcement efficiency and processability of wood fiber-based biocomposites are intimately linked to the morphological and chemical characteristics of the constituent fibers. To elucidate these features for the wood fibers used in this study, a comprehensive suite of microscopy and compositional analyses was conducted.

Fig. 2 presents scanning electron microscopy (SEM) micrographs of the wood fibers at multiple magnifications, alongside quantitative probability density plots for both fiber length and diameter distributions. The SEM images (Fig. 2a, b, d and e) reveal that the wood fibers possess a relatively smooth surface texture and well-preserved cellular structure, which are critical for effective stress transfer within the composite matrix. At higher magnification, the cross-sectional views highlight the integrity of the cell wall architecture, suggesting minimal damage during the pelletization and compounding process.

The diameter distribution (Fig. 2f) follows a normal (Gaussian) profile centered at a mean value of 30.3 μm, with the majority of fibers falling within one standard deviation of the mean. This uniformity is advantageous for composite manufacturing, as it ensures predictable rheological behavior during melt processing and consistent mechanical properties in the final product. In contrast, the fiber length distribution (Fig. 2c) is right-skewed, with a mean length of 0.45 mm. The presence of a substantial fraction of fibers exceeding the mean length contributes to higher aspect ratios, which are known to enhance the reinforcing effect in polymer matrices.

3.1.2 Chemical composition. X-ray photoelectron spectroscopy (XPS) analysis was conducted to characterize the surface chemistry of the wood fibers. The XPS survey spectrum of the wood fibers (Fig. 3a) exhibits characteristic surface elemental composition expected for lignocellulosic materials. The dominant peaks correspond to carbon (C 1s) and oxygen (O 1s), reflecting the prevalence of cellulose, hemicellulose, and lignin at the fiber surface.

High-resolution analysis of the C 1s region (Fig. 3b) reveals the specific carbon environments present at the fiber surface through peak deconvolution into four distinct components. The most intense component (C3) appears at approximately 180 eV binding energy and corresponds to carbon atoms in acetal linkages (O–C–O) and carbonyl groups (C═O), which are characteristic of glycosidic bonds in cellulose and hemicellulose. The C2 component at approximately 160 eV represents carbon atoms bonded to single oxygen atoms (C–O), primarily from hydroxyl groups in cellulose and hemicelluloses. The C4 peak at higher binding energy (~195 eV) is attributed to carboxyl and ester functionalities (O–C═O), while the C1 component at lowest binding energy (~140 eV) corresponds to carbon atoms in C–C and C–H bonds, predominantly from lignin's aromatic and aliphatic structures.

The chemical composition of the wood fibers, determined by monosaccharide analysis (Table 2), is characteristic of soft-

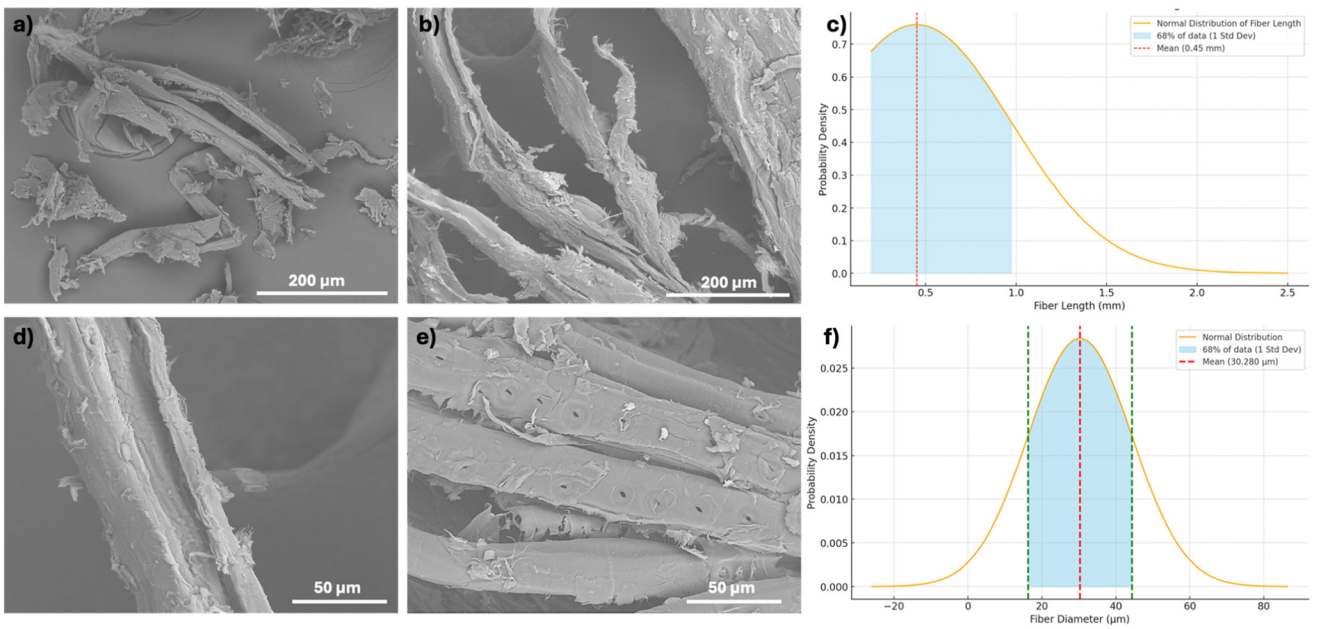

Fig. 2 Morphological characterization and size distribution of the wood fibers. (a and b) SEM micrographs showing the general morphology of the wood fibers. (d and e) Higher magnification SEM images highlighting the surface texture and cross-sectional features of individual fibers. (c) Probability density plot of fiber length distribution, displaying a right-skewed profile with a mean fiber length of 0.45 mm (red dashed line); the shaded blue area represents one standard deviation, encompassing approximately 68% of the measured data. (f) Probability density plot of fiber diameter distribution, illustrating a normal (Gaussian) distribution centered at a mean diameter of 30.3 μm (red dashed line); the blue shaded region denotes one standard deviation from the mean.

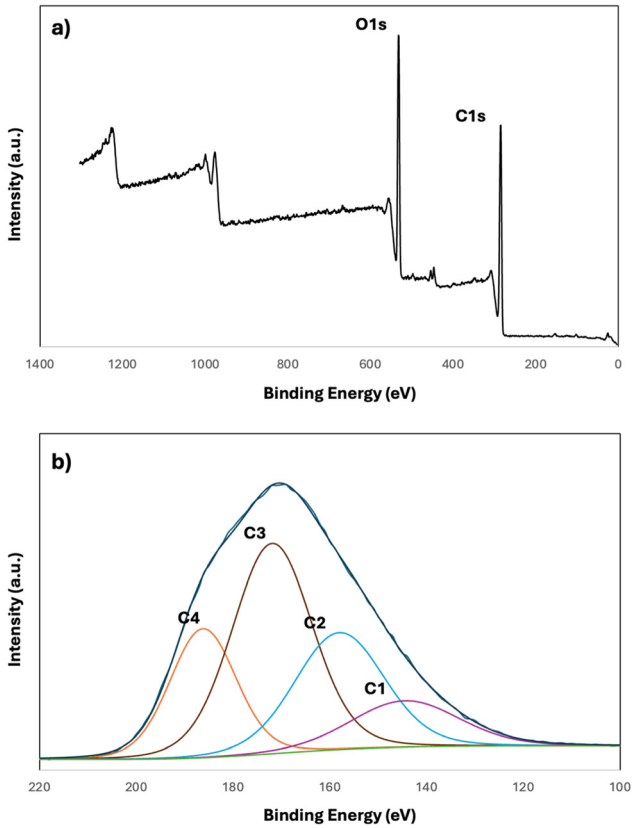

Fig. 3 XPS analysis of the wood fibers. (a) Survey spectrum. (b) High-resolution C 1s spectrum deconvoluted into four carbon environments.

Table 2 Quantitative monosaccharide profile of the wood fibers

Monosaccharide	Concentration (mg g^{-1})	Percentage (%)
Glucose	290.44	71.3
Mannose	64.81	15.9
Xylose	27.09	6.7
Galactose	14.65	3.6
Arabinose	10.10	2.5
Total	407.09	100

wood-derived biomass. Glucose is the predominant sugar (71.3%), reflecting the high cellulose content typical of Norway spruce. Mannose (15.9%) is the major hemicellulosic sugar, primarily present as *O*-acetylgalactoglucomannan, the principal hemicellulose in spruce.[27] The galactose content (3.6%) reflects a substitution degree (Man : Gal ratio) of 4.4 : 1, in agreement with xylose (6.7%) and arabinose (2.5%) are present in lower amounts, representing the typical minor arabinoglucuronoxylan (AGX) component in spruce wood.[28,29]

The dominance of glucose underscores the high cellulose content, which forms the primary load-bearing framework in the wood cell wall and is essential for mechanical reinforcement in composites. The predominance of cellulose confers high tensile strength and stiffness to the fibers, enabling effective load transfer and reinforcement in composite materials. Overall, this composition indicates that the wood fibers are primarily composed of cellulose (reflected by high glucose content), with hemicelluloses – mainly galactoglucomannan – providing a significant secondary fraction. Lignin, while not detected in this monosaccharide analysis, is also expected to be a major component in accordance with typical softwood cell wall composition (approximately 43% cellulose, 35% hemicellulose, and 29% lignin).

3.2. Wood composites

3.2.1 Post-processing morphology and fiber network. Post-processing morphological characterization reveals the preservation of the wood fiber architecture within the PP matrix, a critical factor determining mechanical performance and processing characteristics. Fig. 4 presents optical micrographs of extracted composite sections, demonstrating that individual fibers maintain substantial dimensional integrity despite experiencing high shear forces during twin-screw extrusion and injection molding. Quantitative image analysis confirms fiber lengths ranging from 128 μm to 661 μm post-compounding.

The fiber diameters exhibit stability within the 15–35 μm range after processing, though localized mechanical attrition is evident through diameter variations along individual fibers. These dimensional characteristics position the wood fibers in a positive reinforcement regime, where fiber aspect ratios (length/diameter) are important for load transfer while remaining below lengths that would compromise processability through conventional equipment.

The macroscopic cross-sectional observations (Fig. 5, left panel) and corresponding SEM micrographs (Fig. 5, right panel) reveal the progressive evolution of fiber distribution and network formation with increasing fiber content. Looking at the SEM, it can be seen that at 20 wt% loading, the fibers appear well-dispersed within the PP matrix with minimal agglomeration, maintaining substantial polymer-rich regions between individual fibers. The composite microstructure at this loading exhibits continuous polymer phase reinforced by discrete fibers, allowing for considerable matrix mobility and plastic deformation under mechanical stress.

As fiber content increases to 30 wt%, a more pronounced fiber network emerges, characterized by increased fiber–fiber contacts and reduced polymer-rich regions. This transitional morphology represents a critical threshold where the composite behavior begins to shift from matrix-dominated to fiber-network-dominated. The SEM micrographs clearly demonstrate how fiber proximity increases, creating localized regions where polymer chain mobility becomes significantly restricted. This restriction contributes to the enhanced stiffness observed in mechanical testing while maintaining sufficient matrix continuity for effective stress distribution.

At 50 wt% loading, the microstructure transforms dramatically, presenting a highly entangled, continuous fiber network with substantially diminished polymer-rich regions. The polymer matrix becomes largely confined within the interstices of the fiber network, fundamentally altering the composite's mechanical response. This confined matrix structure impairs

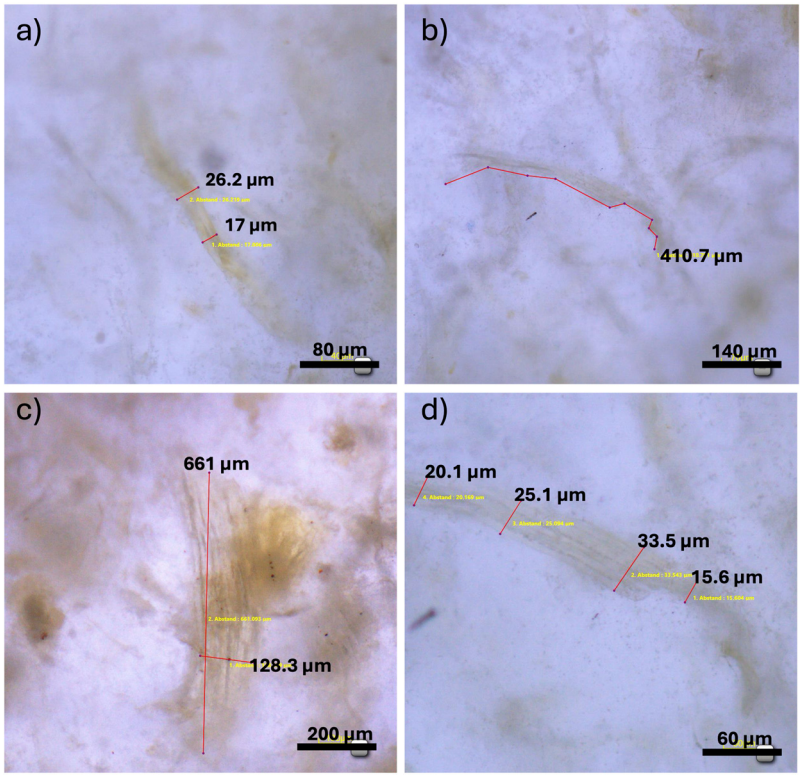

Fig. 4 (a–d) Optical micrographs of wood fibers embedded in the PP matrix after compounding and injection molding.

polymer chain mobility and creates numerous fiber–fiber interfaces that serve as potential stress concentration points. These interfaces often act as crack initiation sites during mechanical loading, particularly under impact conditions, explaining the reduced impact strength observed at higher fiber loadings.

The structural evolution from isolated fiber reinforcement to a continuous fiber network provides a direct morphological explanation for the non-linear mechanical behavior observed in Fig. 7. As polymer–polymer interactions progressively give way to fiber–fiber interactions, the composite transitions from ductile to more brittle behavior, with corresponding gains in stiffness and dimensional stability at elevated temperatures. This fiber network development also accounts for the dramatic reduction in melt flow properties (Fig. 7e), as the entangled fibers create physical barriers to polymer flow during processing.

Three-dimensional micro-computed tomography (µCT) analysis (Fig. 6), performed at the European Synchrotron Radiation Facility, provides deeper insight into the volumetric distribution and orientation of fibers. 3D reconstructions (Fig. 6a) and single-slice tomograms (Fig. 6b) demonstrate effective fiber dispersion across all compositions. Progressive increases of wood fiber volume fractions (Fig. 6c) and fiber–fiber contact and network formation are observed as fiber content rises from 20% to 40%. In particular, the volume fractions of wood fiber extracted from the volumetric data are 20.2 ± 2.4%, 30.8 ± 1.5% and 40.0 ± 2.7% for 20%, 30% and 40% wood fiber content, respectively. Volume analysis also suggests preferential fiber alignment along the flow direction during injection molding.

3.3. Performance of biocomposites

The performance of PP biocomposites reinforced with wood fibers was systematically evaluated as a function of fiber content, with particular emphasis on the balance between mechanical enhancement, processability, and thermal stability (Fig. 7).

As demonstrated in the mechanical property data (Fig. 7a and b), both Young's modulus and tensile strength increase linearly with increasing wood fiber content in PP composites. The data shows a strong linear correlation, confirming that wood fibers effectively reinforce the polymer matrix through efficient stress transfer mechanisms.

This mechanical enhancement is consistent with established structure–property relationships in fiber-reinforced composites, where rigid fibers restrict the deformation of the more flexible polymer matrix. This mechanical enhancement is directly connected to the fiber morphology observed in Fig. 4, where optical micrographs reveal critical dimensional characteristics of wood fibers after compounding. Despite the high shear forces experienced during processing, the fibers maintain significant aspect ratios. Such enhancement in stiffness makes these materials particularly suitable for structural and semi-structural applications where rigidity is critical.

Elongation at break decreases sharply as wood fiber content increases (Fig. 7c), indicating reduced ductility and a tran-

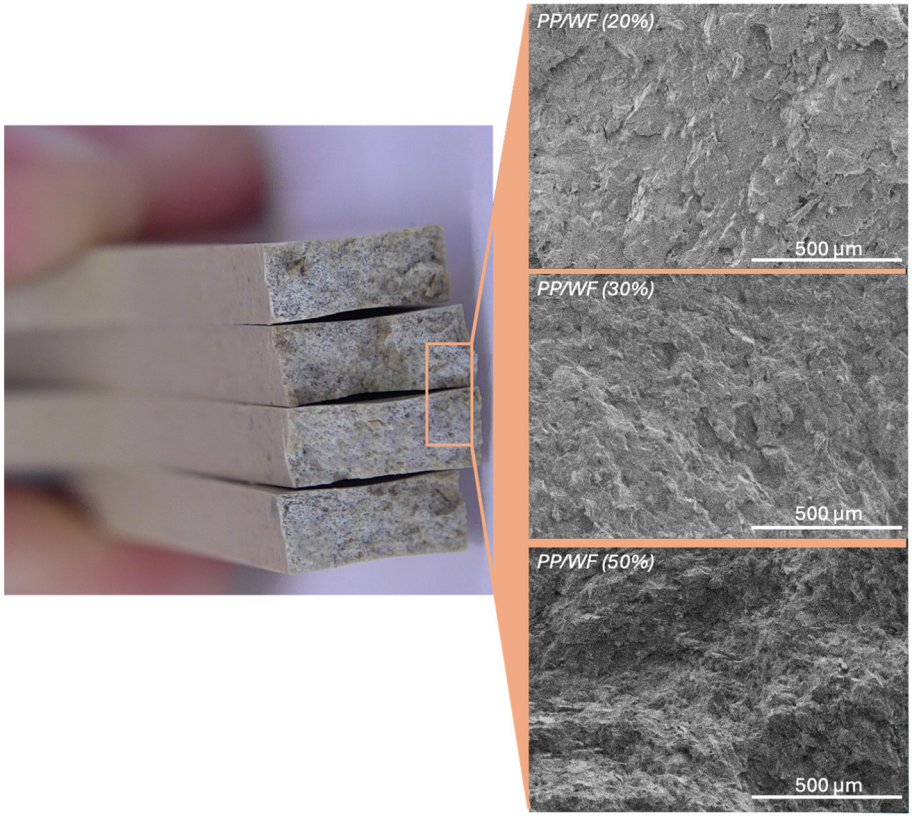

Fig. 5 Macroscopic and microscopic evaluation of the biocomposites' cross-sections at increasing fiber loadings: on the left, cross-sectional photographs of fractured injection-molded PP/WF composite bars containing 20 wt% wood fiber. On the right, SEM micrographs of the composite cross sections with 20, 30 and 50 wt% wood fibers.

sition toward more brittle fracture behavior. This decrease is non-linear, reflecting the complex influence of fiber loading on matrix deformation.

This mechanical behavior fundamentally relates to changes in fiber dispersion with increasing fiber content. As shown in Fig. 6, at 20 wt% loading, discrete and well-dispersed fibers (rendered in red) are separated by continuous polymer regions. These polymer-rich domains allow significant plastic deformation during tensile loading, contributing to relatively high elongation values. At 30 and 50 wt%, a continuous fiber network develops with diminishing polymer-rich regions, altering deformation mechanisms by:

- restricting polymer chain mobility in the bulk matrix;
- creating a mechanically interlocked fiber skeleton that limits matrix flow;
- increasing the number of fiber–matrix interfaces acting as stress concentration points.

Impact strength exhibits a pronounced non-linear decrease with increasing wood fiber content (Fig. 7d), with a tendency to stabilize between 30 and 50 wt% fiber content. This behavior suggests distinct phases in the reduction of toughness, with the rate of decline slowing at higher fiber loadings.

This behavior is associated with the microstructural evolution shown in Fig. 5 and 6, where the tomography and the SEM micrographs reveal the progressive development of a continuous fiber network as wood content increases. At 20 wt% loading, discrete fibers are embedded within a continuous polymer matrix, maintaining sufficient polymer-rich regions for energy absorption through plastic deformation. As fiber content increases to 30 wt%, the emergence of an interconnected fiber network begins to restrict these polymer-rich domains, compromising the composite's ability to dissipate impact energy.

This microstructural transformation fundamentally alters the composite's response to impact loading in two critical ways:

- Each fiber–matrix interface acts as a potential stress concentration site where crack initiation can occur during impact events. The literature suggests that "cracks start in areas with high stress concentration with defects or points, such as areas where the connections between the two phases are very weak".[19,27] As fiber content increases, the number of potential crack initiation sites multiplies exponentially;[30,31]
- The continuous fiber network constrains the polymer matrix's ability to undergo plastic deformation, which is a primary energy absorption mechanism during impact. This restriction is particularly evident in the transition from 30 wt% to higher loadings, where the available polymer-rich regions

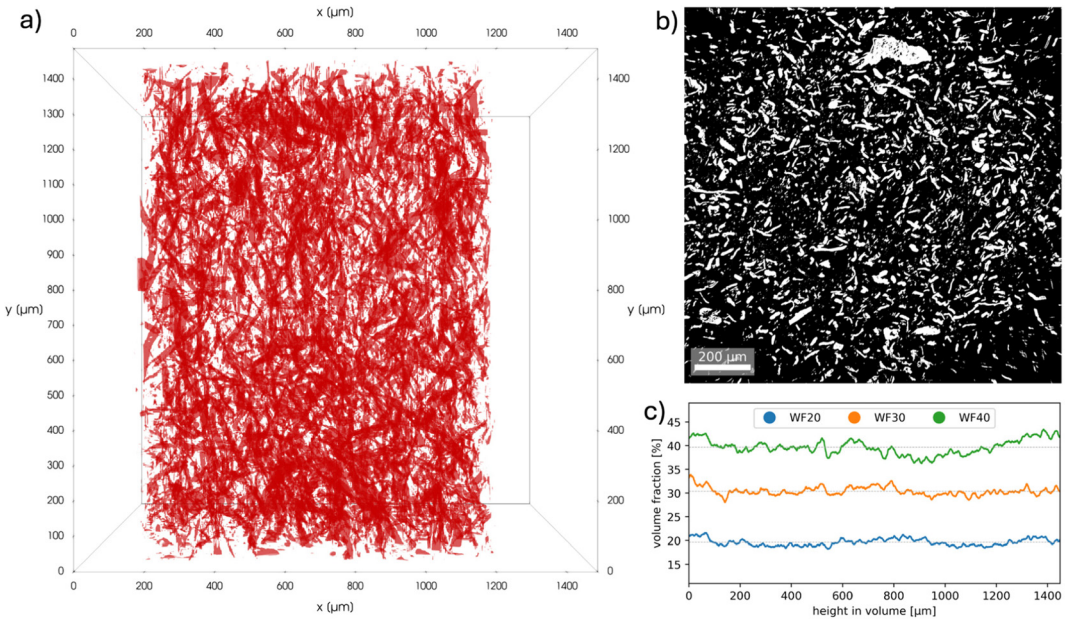

Fig. 6 Three-dimensional micro-computed tomography (µCT) analysis of fiber dispersion in PP/WF biocomposites at varying fiber loadings obtained by phase-contrast tomography at ESRF: (a) 3D rendering of subsampled reconstructed volume after virtual segmentation of wood fiber (red). (b) Tomogram (virtual horizontal slice) through volume from (a): wood fiber in white. Both (a) and (b) illustrate a selected example of injection-molded PP/WF composite with 20 wt% wood fiber content. (c) Variations of wood fiber volume fractions through the height of 3 examples of reconstructed volumes from samples with 20, 30% and 40 wt% wood fiber content, respectively: spatial resolution corresponds to the thickness of each tomogram which is 0.729 µm.

diminish dramatically, as visualized in the cross-sectional SEM micrographs.[15]

The non-linear behaviors shown in Fig. 7 elucidate this behavior, with the inflection point in the curve corresponding to the critical fiber content where the composite transitions from a "matrix-dominated" structure to a "fiber-network-dominated" structure.

The MFI exhibits a pronounced non-linear decrease with increasing wood fiber content (Fig. 7e), following a quadratic relationship. This trend indicates progressively reduced flowability as wood content increases, with virgin PP showing an MFI value of approximately 43 g per 10 min that drops dramatically to below 5 g per 10 min at 50 wt% wood loading. This behavior aligns with established polymer composite theory, where rigid fillers restrict polymer chain mobility and create additional resistance to flow. The non-linear nature of the MFI reduction can be attributed to two competing effects: at lower wood content (below 20 wt%), the primary mechanism is disruption of polymer chain mobility by individual fibers, while at higher loadings (30–50 wt%), fiber–fiber interactions become increasingly dominant, causing a more pronounced viscosity increase. This is consistent with observations in the microscopy and tomography analyses (Fig. 4 and 6), where higher fiber loadings show increasingly interconnected fiber networks.

The VICAT B softening temperature increases linearly with wood fiber content (Fig. 7f). This proportional enhancement in thermal resistance is highly advantageous for applications requiring dimensional stability at elevated temperatures. The unfilled PP exhibits a VICAT B temperature of approximately 64 °C, which increases to 82 °C at 30 wt% wood loading and surpasses 105 °C at 50 wt% fiber content. This improvement in thermal resistance correlates with the formation of a rigid fiber network within the matrix, which physically restricts polymer chain mobility and delays the onset of softening.

3.4. Recyclability of biocomposites

The recyclability of biocomposites represents one of the most critical challenges for their widespread adoption in a circular economy framework. Despite their environmental advantages in terms of renewable content and reduced carbon footprint, biocomposites face significant barriers to effective end-of-life management due to insufficient recycling infrastructure and underdeveloped sorting streams. As the plastic industry transitions toward sustainability, recycling has been seen as one of the most important efforts to mitigate the environmental effects of plastics, yet biocomposites often fall outside existing recycling systems designed primarily for conventional polymers. Addressing these recycling challenges is essential not only for minimizing waste but also for optimizing the resource efficiency of biocomposites, particularly as they represent a promising pathway for valorizing industrial side-streams and reducing dependence on virgin materials.

To systematically evaluate the recyclability of PP/WF biocomposites, a comprehensive closed-loop assessment protocol was implemented, as illustrated in Fig. 8a. This experimental

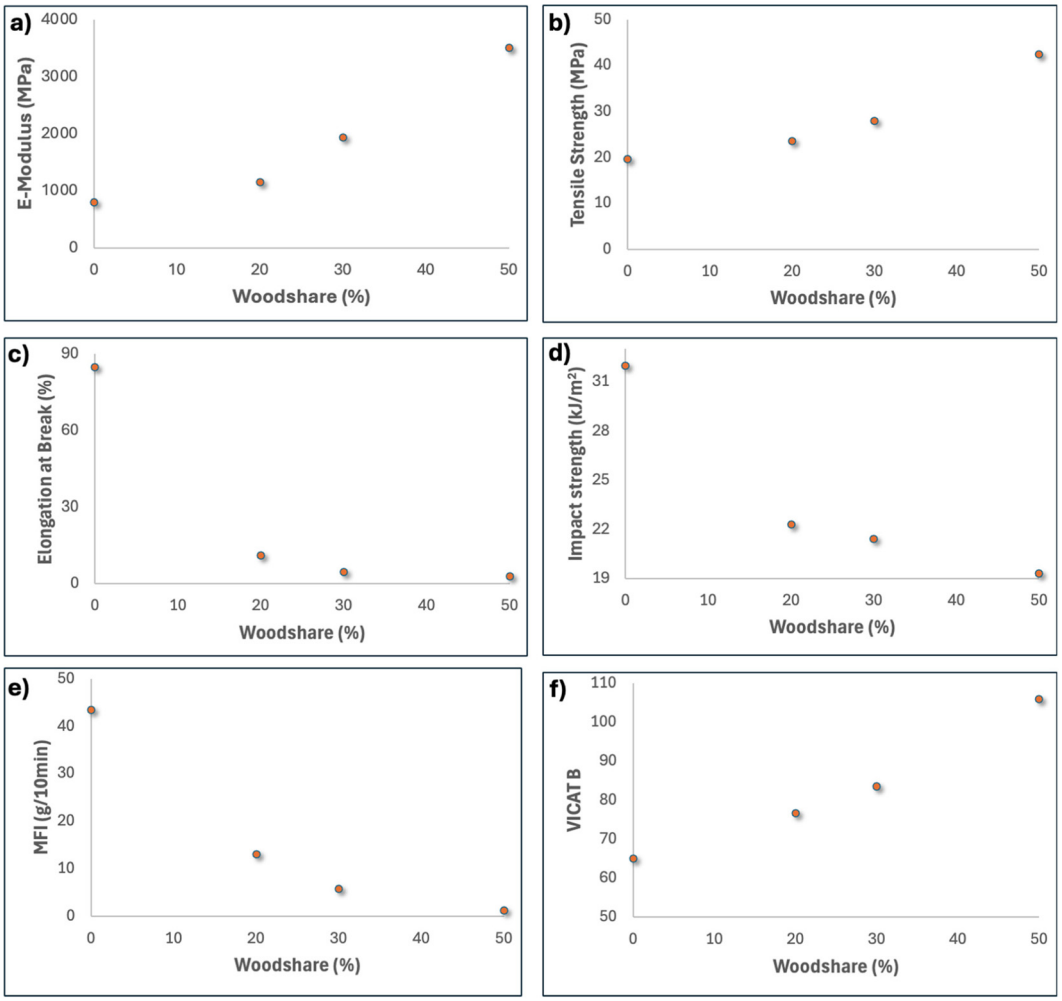

Fig. 7 Effect of wood fiber content on the mechanical, thermal, and processing properties of PP/WF biocomposites fitted trendline and regression equation: (a) Young's modulus, (b) tensile strength, (c) elongation at break, (d) impact strength (Charpy, notched), (e) melt flow index, (f) VICAT B; as a function of wood fiber content.

approach involved subjecting the materials to three complete processing cycles, each consisting of mechanical testing, shredding of test specimens, re-compounding, and re-injection molding into standardized test specimens. This methodology simulates industrial recycling conditions while enabling precise tracking of property evolution. It is noteworthy that exclusively biocomposite with 20 wt% WF was used for this recycling evaluation.

Fig. 8b provides visual evidence of the physical changes occurring during multiple recycling cycles for both virgin PP and PP/WF composites. The virgin PP samples (bottom row) exhibit a progressive yellowing transition after each processing cycle. This chromatic shift indicates thermal-oxidative degradation of the PP matrix itself, resulting from chain scission and the formation of carbonyl groups during repeated high-temperature processing. The PP/WF composites (top row) transitioned from light brown to significantly darker brown after three recycling cycles. While this darkening is partially attributable to thermal degradation of lignin components within the wood fibers, the PP matrix contributes substantially to the overall darkening.

The comprehensive mechanical property data presented in Table 3 quantitatively demonstrates the superior recyclability performance of PP/WF biocomposites compared to virgin PP. The biocomposite maintains tensile strength stability, declining from 23.50 MPa to 22.20 MPa after three cycles (94.5% retention), while virgin PP degrades from 19.70 MPa to 18.50 MPa (93.9% retention). Most remarkably, elongation at break behavior reveals fundamental differences: PP/WF stabilizes around 7–10% after initial reduction, whereas virgin PP experiences catastrophic ductility loss from 85% to 16% (81.2% decline). The flexural modulus data confirms PP/WF's structural integrity with 92.9% retention (3424 to 3180 MPa) *versus* PP's severe degradation to 58.7% retention (3921 to 2303 MPa), directly demonstrating the fiber network's stabilizing effect during repeated processing.

The mechanical recyclability assessment of PP/WF biocomposites (Fig. 8c–f) reveals a compelling pattern of property

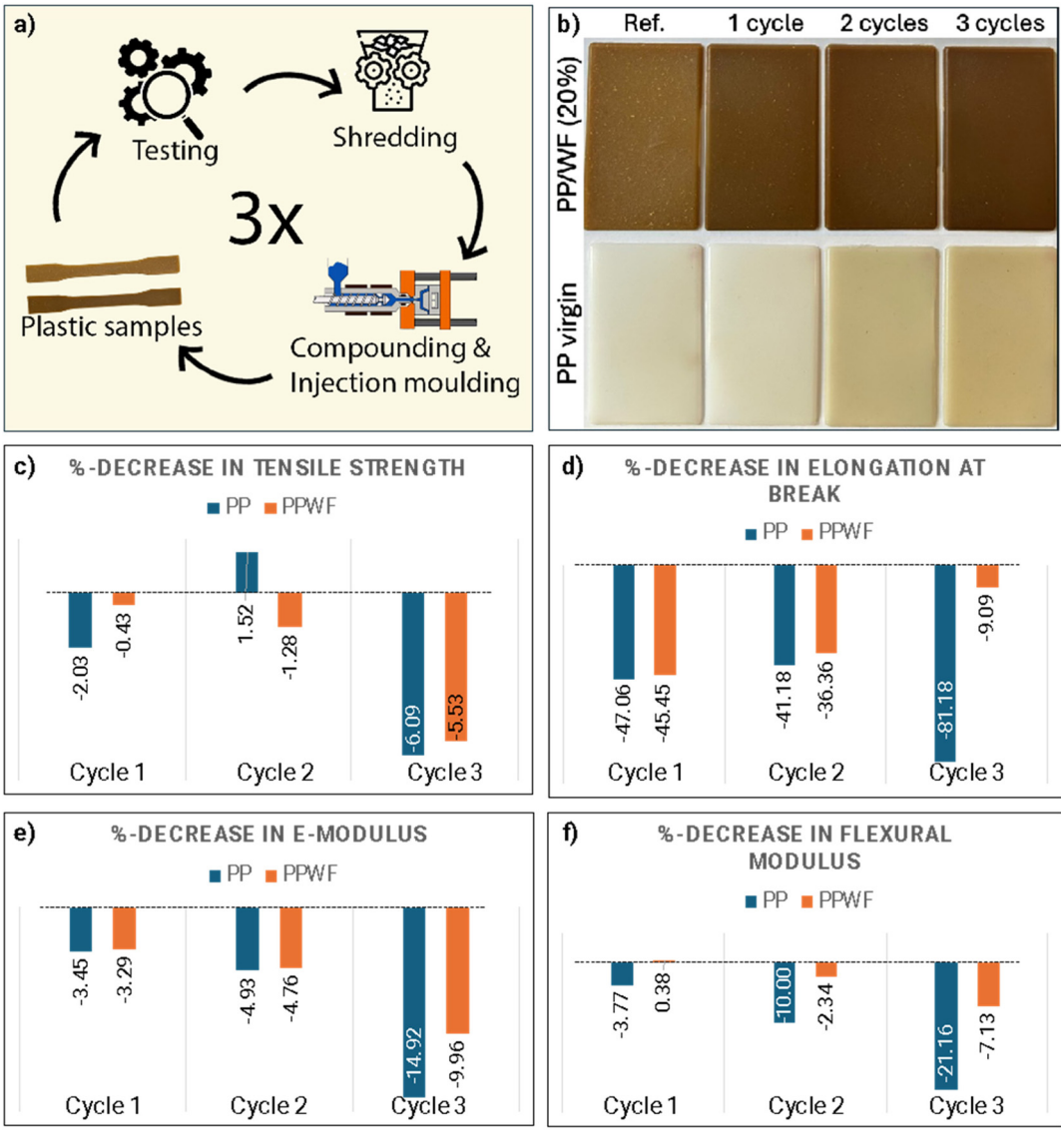

Fig. 8 Mechanical recyclability assessment of PP/WF biocomposites compared to virgin PP. (a) Schematic overview of the closed-loop recycling protocol. (b) Representative images of injection-molded plates for PP/WF (20 wt%) and virgin PP after 0 (reference), 1, 2, and 3 recycling cycles. (c–f) Bar graphs showing the percentage decrease in key mechanical properties of PP and PP/WF after each recycling cycle: (c) tensile strength, (d) elongation at break, (e) Young's modulus (*E*-modulus) and (f) flexural modulus.

Table 3 Mechanical and processing properties of PP/WF (20 wt%) biocomposites and virgin PP through multiple recycling cycles

Sample	Tensile strength (MPa)	Tensile modulus (MPa)	Elongation at break (%)	Impact strength (ft·lbf/in)	Flexural modulus (MPa)	MFI (g per 10 min)
PP/WF	23.50	1155.00	11	1.37	3424.00	13.00
1 cycle	23.40	1117.00	6	1.35	3437.00	14.60
2 cycles	23.20	1100.00	7	1.19	3344.00	14.22
3 cycles	22.20	1040.00	10	1.24	3180.00	18.84
PP	19.70	811.00	85	1.97	2921.00	43.38
1 cycle	19.30	783.00	45	2.08	2811.00	48.70
2 cycles	21.40	771.00	50	2.81	2629.00	47.80
3 cycles	18.50	690.00	16	3.23	2303.00	39.80

retention compared to virgin PP. Examining the data in detail, tensile strength degradation follows similar trajectories for both materials, with virgin PP showing steady deterioration (−2.03%, −1.52%, and −6.09% across cycles 1–3) while PP/WF exhibits minimal initial decline (−0.43%), a slight dip in cycle 2 (−1.28%), before converging with PP at approximately −5.5% by cycle 3. This suggests that fiber–matrix interface integrity remains largely preserved throughout recycling. More dramatic differences emerge in elongation at break (Fig. 8d), where both materials initially lose approximately 45–47% after the first cycle but diverge significantly thereafter. By the third cycle, virgin PP experiences substantial ductility loss (−81.18%) while the biocomposite shows an initial drop from 11% to 6%, then stabilizes around 7–10% in subsequent cycles, representing better relative stability after initial processing-induced changes.

Young's modulus (*E*-modulus) deteriorates more gradually for PP/WF than virgin PP, culminating in superior retention after three cycles (−9.96% *vs.* −14.52%). Most remarkable is the flexural modulus behavior, where PP/WF actually exhibits property improvement after the first recycling cycle (+0.38%) before minimal degradation in subsequent cycles. This unexpected enhancement may result from improved fiber alignment and distribution during reprocessing, creating more effective load transfer pathways. Meanwhile, virgin PP shows consistent flexural property decline across all cycles (−3.77%, −10.00%, and −22.16%). Impact strength behavior reveals contrasting trends: PP/WF shows a slight decrease from 1.37 to 1.24 ft·lbf/in (−9.5%), while virgin PP paradoxically increases from 1.97 to 3.23 ft·lbf/in (+64%). This reflects an inverse relationship between stiffness and impact toughness in degraded thermoplastics, potentially due to shorter polymer chains that exhibit reduced stiffness but enhanced ductility and impact absorption capacity.

Thermogravimetric analysis (TGA) and derivative thermogravimetry (DTG) curves (Fig. 9a–e) provide clear evidence of

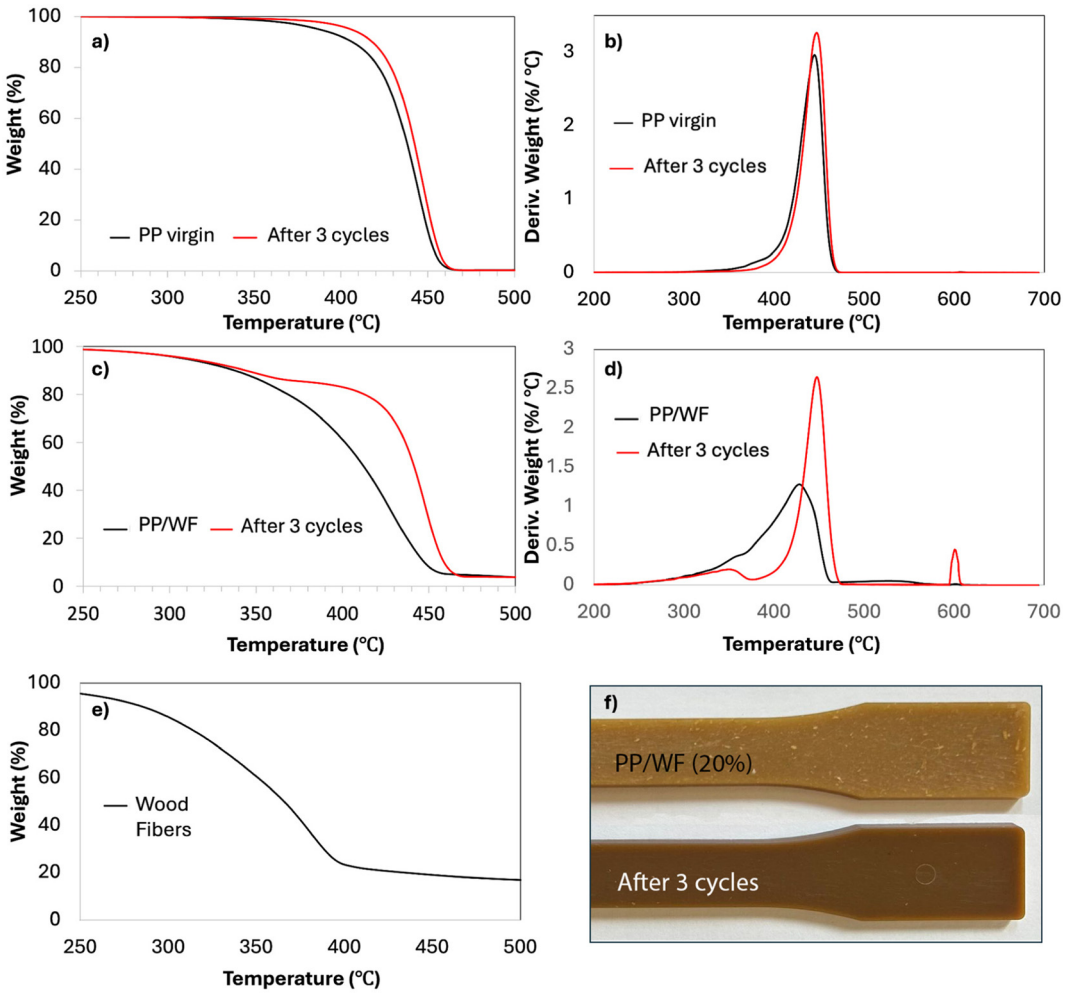

Fig. 9 Thermal stability for PP/WF biocomposites and reference materials before and after mechanical recycling cycles: (a and b) TGA and derivative TGA (DTG) curves for virgin PP before and after three recycling cycles. (c and d) TGA and DTG curves for PP/WF (20 wt% wood fiber) composites before and after three recycling cycles. (e) TGA curve for wood fibers alone. (f) Photographs of PP/WF (20 wt%) dogbone specimens before and after three recycling cycles.

the thermal stability of both virgin PP and PP/WF biocomposites after three mechanical recycling cycles. For virgin PP (Fig. 9a and b), the onset and peak decomposition temperatures show only a minor shift after repeated processing, indicating that the polymer matrix retains its core thermal resistance even after multiple cycles.

The PP/WF composites (Fig. 9c and d) display a characteristic two-step degradation profile. Notably, after three recycling cycles (red line), the degradation curve shifts substantially to higher temperatures compared to the virgin composite (black line), demonstrating markedly improved thermal stability. This enhancement is particularly evident in Fig. 9d, where the DTG peaks for the recycled composite appear at higher temperatures and with different peak intensities compared to the virgin material.

The comparison with the TGA curve for the wood fibers alone (Fig. 9e) highlights that while wood fibers inherently begin degrading at lower temperatures than the polymer matrix, their integration into the composite-and particularly after multiple recycling cycles-creates a synergistic effect that enhances overall thermal resistance.

This improved thermal stability correlates directly with the visual evidence in Fig. 9f, where the specimens after three cycles show a more uniform appearance. This suggests better fiber dispersion and embedding within the matrix after repeated processing. Previous works have demonstrated that better dispersion of the wood fibers creates a more thermally stable composite structure.[32]

The thermal properties of virgin PP and PP/WF composites before and after three mechanical recycling cycles were evaluated by differential scanning calorimetry (DSC), as presented in Fig. 10 and Table 4. For virgin PP, the DSC thermogram prior to recycling exhibited a single, sharp melting peak at 163.4 °C with a corresponding enthalpy of fusion of 80.17 J g^{-1}, indicative of a well-defined crystalline structure. After three recycling cycles, the PP sample displayed a notable change in melting behavior, characterized by the emergence of two distinct melting peaks at 129.1 °C and 160.0 °C. This splitting of the melting peak suggests the formation of less perfect or smaller crystallites, likely resulting from polymer chain scission and partial recrystallization during repeated processing. The degree of crystallinity for PP dropped from 38.4% to 31.2% after recycling, and the crystallization temperature decreased from 122.4 °C to 116.9 °C, reflecting reduced chain regularity and mobility.

For the PP/WF composite, the thermal behavior after recycling demonstrated complex crystalline reorganization compared to neat PP. Before recycling, the composite exhibited a main melting peak at 162.6 °C, which shifted only minimally to 161.2 °C after three recycling cycles, a reduction of merely 1.4 °C. While additional minor peaks appeared at 124.1 °C

Table 4 DSC thermal properties of virgin PP and PP/WF (20 wt%) composites before and after three mechanical recycling cycles

Sample	Melting temperature (T_m) – °C	Crystallization temperature (T_c) – °C	Crystallinity degree (X_c) – %
PP (0 cycles)	163.45	122.38	38.4
PP (3 cycles)	129.10, 160.04	116.90	31.2
PP/WF (0 cycles)	162.6	120.59	39.0
PP/WF (3 cycles)	161.22	120.88	21.5

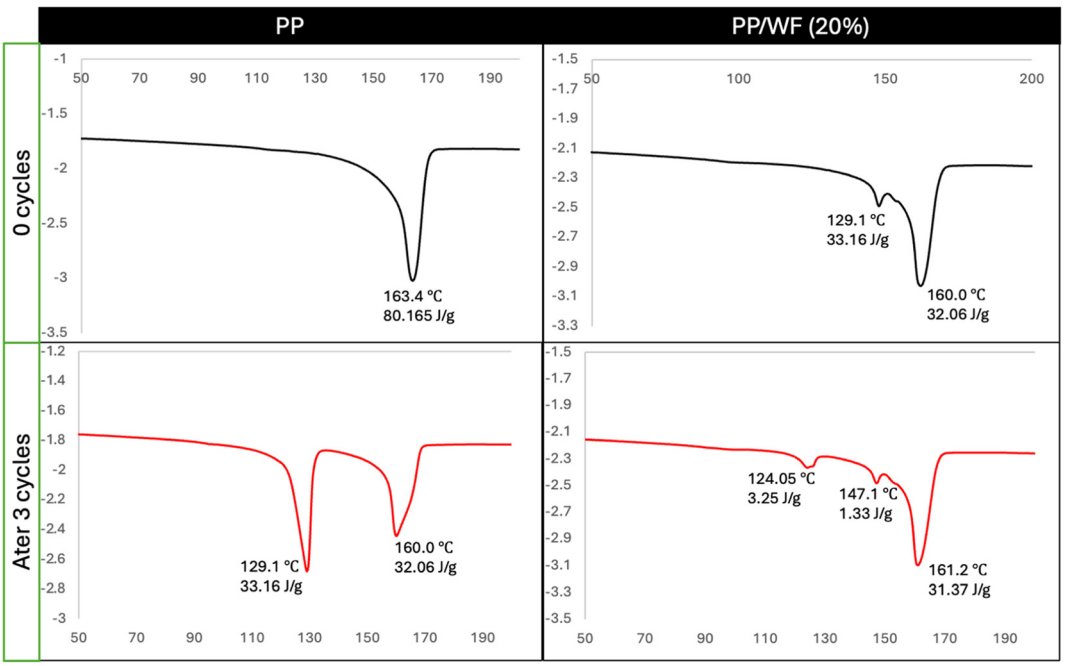

Fig. 10 DSC thermograms: DSC of virgin PP and PP/WF (20 wt%) composites before and after three mechanical recycling cycles.

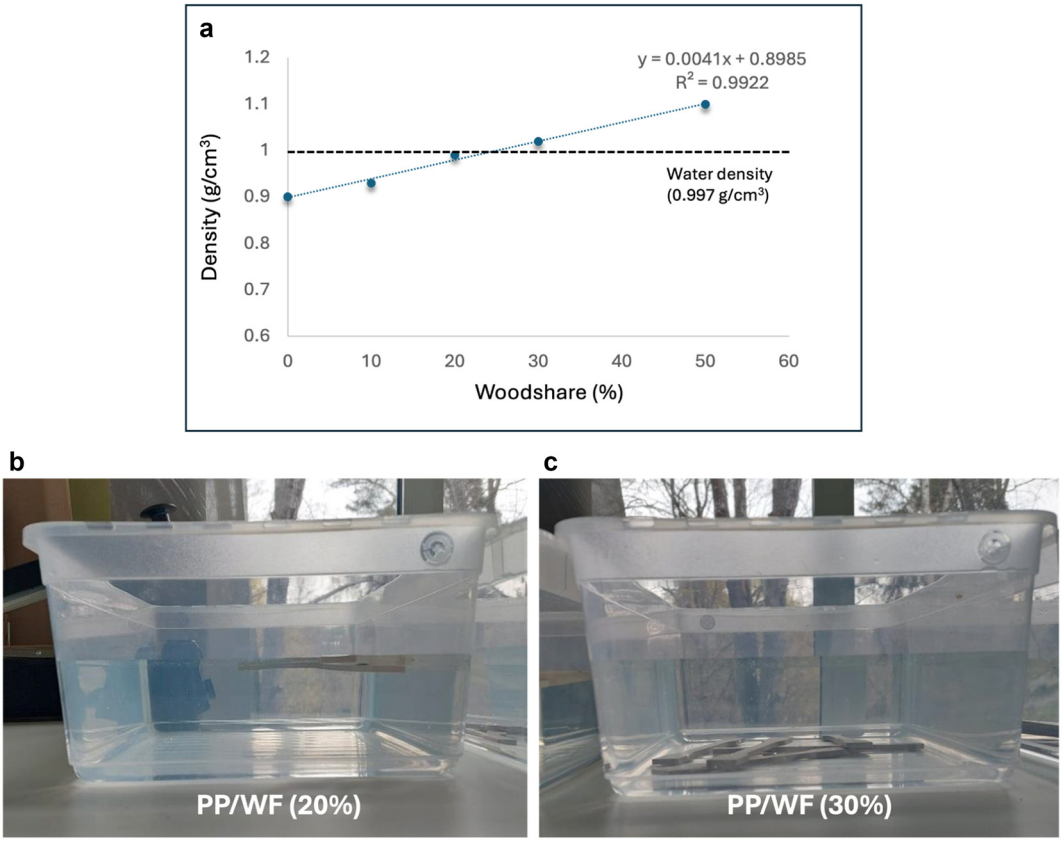

Fig. 11 Density-based flotation behavior of PP/WF biocomposites: (a) correlation between wood fiber content and density. (b and c) Photographic sequence showing floating (PP02-20, 20 wt% wood fiber) and sinking (PP02-30) biocomposite specimens in water.

and 147.1 °C after recycling, indicating some reorganization of the crystalline structure, the primary melting transition remained remarkably stable. However, the degree of crystallinity in the PP/WF composite decreased substantially from 39% to 21.5%, representing a more significant disruption compared to virgin PP (38.4% to 31.2%). This greater crystallinity loss in the biocomposite likely reflects the interference of wood fibers with polymer chain reorganization during repeated processing cycles.

Despite this crystallinity reduction, the preservation of the main melting temperature and the maintenance of mechanical properties suggest that the fiber network provides alternative load-bearing pathways that compensate for reduced crystalline organization. The wood fibers appear to create a reinforcing skeleton that maintains composite integrity even as the polymer matrix experiences thermal degradation, resulting in overall superior property retention compared to the unreinforced polymer matrix.

Furthermore, the flotation behavior of these biocomposites reveals a critical transition in density-based separation potential. As seen in Fig. 11, materials containing 20% wood fibers maintain buoyancy (density 0.98 g cm^{-3}) while those with 30% wood fiber content sink, indicating that the practical density threshold for water-based separation lies between these two compositions. This transition point enables efficient separation from higher-density plastics using existing sink-float recycling infrastructure, facilitating the development of dedicated recycling streams for wood-plastic composites with fiber contents at or below 20 wt%.

4. Conclusions

This work rigorously demonstrates that polypropylene composites reinforced with wood fibers (FibraQ) exhibit marked improvements in mechanical and thermal properties directly correlated to fiber loading and microstructural evolution. Quantitative monosaccharide analysis confirms the fibers' biochemical integrity with cellulose, galactoglucomannan and arabinoglucuronoxylan dominating as main polysaccharide components in spruce wood, underpinning effective reinforcement. Microscopy and synchrotron μCT reveal that fiber dimensions and dispersion remain well preserved post-processing, enabling the critical formation of a continuous fiber network above 30 wt% loading. This network formation drives linear increases in tensile modulus and strength, accompanied by nonlinear reductions in ductility and impact toughness due to constrained polymer mobility and increased fiber–matrix interface density. Thermal characterization affirms that these composites gain enhanced thermal stability and elevated Vicat

softening temperatures with fiber addition, crucial for high-temperature applications. Closed-loop mechanical recycling over three cycles shows more consistent retention of mechanical properties—including impact toughness—than neat PP, indicating the fiber network's stabilizing effect during repeated processing. Moreover, density-driven flotation tests establish a practical sorting window for recycling stream separation around 24 wt% fiber content, supporting industrial-scale recoverability.

Conflicts of interest

There are no conflicts to declare.

Data availability

All relevant data supporting the findings of this study are included within the main article. Additional datasets related to this work are available from the corresponding author upon reasonable request.

Acknowledgements

The authors thank financial support of the Vinnova through the project 2021-03832. We acknowledge the European Synchrotron Radiation Facility (ESRF) for provision of synchrotron radiation facilities, and we would like to thank Philip Cook for assistance and support in using beamline BM05.

References

1 H. Ritchie, V. Samborska and M. Roser, "Plastic Pollution", Published online at OurWorldinData.org, 2023. Available at: https://ourworldindata.org/plastic-pollution [accessed 2025].
2 Plastics – the fast Facts 2024. Available at: https://plasticseurope.org/knowledge-hub/plastics-the-fast-facts-2024/ [accessed 2025].
3 Annual production of plastics worldwide from 1950 to 2023. Available at: https://www.statista.com/statistics/282732/global-production-of-plastics-since-1950/ [accessed 2025].
4 B. P. S. Gautam, A. Qureshi, A. Gwasikoti, V. Kumar and M. Gondwal, Global Scenario of Plastic Production, Consumption, and Waste Generation and Their Impacts on Environment and Human Health, in *Advanced Strategies for Biodegradation of Plastic Polymers*, ed. R. Soni, P. Debbarma, D. C. Suyal and R. Goel, Springer, Cham, 2024, DOI: 10.1007/978-3-031-55661-6_1.
5 T. Davidson, How much plastic actually gets recycled?, 2024. Available at: https://blog.cleanhub.com/how-much-plastic-is-recycled [accessed 2025].
6 H. Albert, Less than 10% of plastics are produced using recycled materials, Chemistry World News, 2025. Available at: https://www.chemistryworld.com/news/less-than-10-of-plastics-are-produced-using-recycled-materials/4021407.article [accessed 2025].
7 U. Salahuddin, J. Sun, C. Zhu, M. Wu, B. Zhao and P.-X. Gao, Plastic Recycling: A Review on Life Cycle, Methods, Misconceptions, and Techno-Economic Analysis, *Adv. Sustainable Syst.*, 2023, **7**(7), 2200471, DOI: 10.1002/adsu.202200471.
8 M. G. Kibria, N. I. Masuk, R. Safayet, H. Q. Nguyen and M. Mourshed, Plastic Waste: Challenges and Opportunities to Mitigate Pollution and Effective Management, *Int. J. Environ. Res.*, 2023, **17**(1), 20, DOI: 10.1007/s41742-023-00507-z.
9 E. Naderi Kalali, S. Lotfian, M. Entezar Shabestari, S. Khayatzadeh, C. Zhao and H. Yazdani Nezhad, A critical review of the current progress of plastic waste recycling technology in structural materials, *Curr. Opin. Green Sustainable Chem.*, 2023, **40**, 100763, DOI: 10.1016/j.cogsc.2023.100763.
10 M. Mujtaba, L. Fraceto, M. Fazeli, S. Mukherjee, S. Savassa, G. Araujo de Medeiros, A. do E. Santo Pereira, S. Donnini Mancini, J. Lipponen and F. Vilaplana, Lignocellulosic biomass from agricultural waste to the circular economy: A review with focus on biofuels, biocomposites and bioplastics, *J. Cleaner Prod.*, 2023, **402**, 136815, DOI: 10.1016/j.jclepro.2023.136815.
11 P. Sanna, K. Harri and A. Antti, Recovery rates of logging residue harvesting in Norway spruce (Picea abies (L.) Karsten) dominated stands, *Biomass Bioenergy*, 2011, **35**(4), 1545–1551, DOI: 10.1016/j.biombioe.2010.12.032.
12 Natural Fiber Composites Market Trends. Available at: https://www.grandviewresearch.com/industry-analysis/natural-fiber-composites-market [accessed 2025].
13 S. Manabendra, S. Hari, S. M. Kumar, S. M. Rangappa and S. Suchart, Advancements in natural fiber composites: Market insights, surface modifications, advanced fabrication techniques and applications, *Sustainable Chem. Clim. Action*, 2025, **6**, 100081, DOI: 10.1016/j.scca.2025.100081.
14 M. De Schoenmakere and Y. Hoogeveen, The circular economy and the bioeconomy - Partners in sustainability, European Environment Agency (EEA) Report No 8/2018, 2018, DOI: 10.2800/02937.
15 J. L. Thomason and J. L. Rudeiros-Fernández, A Review of the Impact Performance of Natural Fiber Thermoplastic Composites, *Front. Mater.*, 2018, **5**, 60, DOI: 10.3389/fmats.2018.00060.
16 P. H. P. M. da Silveira, M. C. C. d. Santos, Y. S. Chaves, M. P. Ribeiro, B. Z. Marchi, S. N. Monteiro, A. V. Gomes, N. d. L. C. O. Tapanes, P. S. d. C. Pereira and D. C. Bastos, Characterization of Thermo-Mechanical and Chemical Properties of Polypropylene/Hemp Fiber Biocomposites: Impact of Maleic Anhydride Compatibilizer and Fiber Content, *Polymers*, 2023, **15**, 3271, DOI: 10.3390/polym15153271.
17 M. Baig, B. Almeshari, A. Aabid, H. Junaedi and A. Almajid, The effect of maleic anhydride grafted polypropylene addition on the degradation in the mechanical properties

of the PP/wood composites, *Heliyon*, 2024, **10**(9), e30510, DOI: 10.1016/j.heliyon.2024.e30510.

18 J. Neto, H. Queiroz, R. Aguiar, R. Lima, D. Cavalcanti and M. D. Banea, A Review of Recent Advances in Hybrid Natural Fiber Reinforced Polymer Composites, *J. Renewable Mater.*, 2022, **10**(3), 561–589, DOI: 10.32604/jrm.2022.017434.

19 A. D. Nugraha, M. I. Nuryanta, L. Sean, K. Budiman, M. Kusni and M. A. Muflikhun, Recent Progress on Natural Fibers Mixed with CFRP and GFRP: Properties, Characteristics, and Failure Behaviour, *Polymers*, 2022, **14**, 5138, DOI: 10.3390/polym14235138.

20 M. Slamani and J. F. Chatelain, A review on the machining of polymer composites reinforced with carbon (CFRP), glass (GFRP), and natural fibers (NFRP), *Discover Mech. Eng.*, 2023, **2**, 4, DOI: 10.1007/s44245-023-00011-w.

21 X. Zhao, Y. Liu, Z. Li and H. Chen, Recycling of natural fiber composites: Challenges and opportunities, *Resour., Conserv. Recycl.*, 2022, **177**, 105962, DOI: 10.1016/j.resconrec.2021.105962.

22 X. Zhao, Y. Liu, Z. Li and H. Chen, Recycling of natural fiber composites: Challenges and opportunities, *Resour., Conserv. Recycl.*, 2022, **177**, 105962, DOI: 10.1016/j.resconrec.2021.105962.

23 C. Branfoot, R. J. K. Taylor and T. Hasell, Recovery of chemical recyclates from fibre-reinforced composites by solvolysis, *Polymer*, 2023, **285**, 126362, DOI: 10.1016/j.polymer.2023.126362.

24 C. Branfoot, R. J. K. Taylor and T. Hasell, Recovery of chemical recyclates from fibre-reinforced composites by solvolysis, *Polymer*, 2023, **285**, 126362, DOI: 10.1016/j.polymer.2023.126362.

25 FibraQ, Lowering carbon footprints. Available at: https://www.fibra-q.com/ [accessed 2025].

26 S. Matthis, Sweden first in the world to 3D print one-piece bio-based kayak, 2022. Available at: https://www.pulpapernews.com/20220705/13709/sweden-first-world-3d-print-one-piece-bio-based-kayak [accessed 2025].

27 M. Berglund, R. Jiménez-Barbero and P. T. Larsson, Isolation and characterization of O-acetyl-galactoglucomannan from spruce (Picea abies) chips, *Carbohydr. Polym.*, 2002, **48**, 29–39, DOI: 10.1016/S0144-8617(01)00210-7.

28 A. Martinez-Abad, J. Berglund, G. Toriz, P. Gatenholm, G. Henriksson, M. Lindstrom, J. Wohlert and F. Villaplana, Regular Motifs in Xylan Modulate Molecular Flexibility and Interactions with Cellulose Surfaces, *Plant Physiol.*, 2017, **175**, 1579–1592, DOI: 10.1104/pp.17.01184.

29 W. Zhang, X. Hu, H. Xiang and X. Zhu, Influence of the molecular motifs of mannan and xylan on the enzymatic saccharification of lignocellulosic biomass, *Green Chem.*, 2020, **22**, 3956–3970, DOI: 10.1039/d0gc01207f.

30 F. Lopez-Jimnez, Numerical Modeling of Stress Concentration around Failed Fibers in Unidirectional Composites, AIAA SciTech Forum, 2021, 1–10, DOI: 10.2514/6.2021-0087.

31 H. Khademieslam and M. Kalagar, Evaluation of the bending strength, impact strength, and morphological properties of wheat straw fiber/paper mill sludge/polypropylene composites, *BioRes.*, 2016, **11**(2), 3914–3922, DOI: 10.15376/biores.11.2.3914-3922.

32 L. Rosenstock Völtz, I. Di Guiseppe, S. Geng and K. Oksman, The Effect of Recycling on Wood-Fiber Thermoplastic Composites, *Polymers*, 2020, **12**, 1750, DOI: 10.3390/polym12081750.